Article

# Normal Mode Analysis of *Pyrococcus furiosus* Rubredoxin via Nuclear Resonance Vibrational Spectroscopy (NRVS) and Resonance Raman Spectroscopy

Yuming Xiao, Hongxin Wang, Simon J. George, Matt C. Smith, Michael W. W. Adams, Francis E. Jenney,, Wolfgang Sturhahn, Ercan E. Alp, Jiyong Zhao, Y. Yoda, Abishek Dey, Edward I. Solomon, and Stephen P. Cramer

*J. Am. Chem. Soc.*, **2005**, 127 (42), 14596-14606• DOI: 10.1021/ja042960h • Publication Date (Web): 04 October 2005



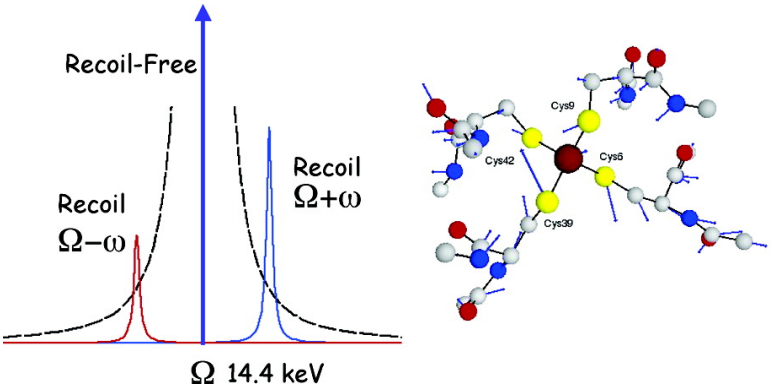


## More About This Article

Additional resources and features associated with this article are available within the HTML version:

- Supporting Information
- Links to the 7 articles that cite this article, as of the time of this article download
- Access to high resolution figures
- Links to articles and content related to this article
- Copyright permission to reproduce figures and/or text from this article

View the Full Text HTML

J|A|C|S
ARTICLES
Published on Web 10/04/2005

# Normal Mode Analysis of *Pyrococcus furiosus* Rubredoxin via Nuclear Resonance Vibrational Spectroscopy (NRVS) and Resonance Raman Spectroscopy

Yuming Xiao,[†] Hongxin Wang,[‡] Simon J. George,[‡] Matt C. Smith,[†] Michael W. W. Adams,[||] Francis E. Jenney, Jr.,[||] Wolfgang Sturhahn,[⊥] Ercan E. Alp,[⊥] Jiyong Zhao,[⊥] Y. Yoda,[#] Abishek Dey,[§] Edward I. Solomon,[§] and Stephen P. Cramer*[,†,‡]

*Contribution from the Department of Applied Science, University of California, Davis, California 95616, Physical Biosciences Division, Lawrence Berkeley National Laboratory, Berkeley, California 94720, Department of Chemistry, Stanford University, Stanford, California 94305, Department of Biochemistry and Molecular Biology, University of Georgia, Athens, Georgia 30602, Advanced Photon Source, Argonne National Laboratory, Argonne, Illinois 60439, and JASRI, SPring-8, 1-1-1 Kouto, Mikazuki-cho, Sayo-gun, Hyogo 679-5198, Japan*

Received November 22, 2004; E-mail: spcramer@ucdavis.edu

***Abstract:*** We have used $^{57}$Fe nuclear resonance vibrational spectroscopy (NRVS) to study the $Fe(S_{cys})_4$ site in reduced and oxidized rubredoxin (Rd) from *Pyrococcus furiosus* (*Pf*). The oxidized form has also been investigated by resonance Raman spectroscopy. In the oxidized Rd NRVS, strong asymmetric Fe−S stretching modes are observed between 355 and 375 cm$^{-1}$; upon reduction these modes shift to 300−320 cm$^{-1}$. This is the first observation of Fe−S stretching modes in a reduced Rd. The peak in S−Fe−S bend mode intensity is at ∼150 cm$^{-1}$ for the oxidized protein and only slightly lower in the reduced case. A third band occurs near 70 cm$^{-1}$ for both samples; this is assigned primarily as a collective motion of entire cysteine residues with respect to the central Fe. The $^{57}$Fe partial vibrational density of states (PVDOS) were interpreted by normal mode analysis with optimization of Urey−Bradley force fields. The three main bands were qualitatively reproduced using a $D_{2d}$ $Fe(SC)_4$ model. A $C_1$ $Fe(SCC)_4$ model based on crystallographic coordinates was then used to simulate the splitting of the asymmetric stretching band into at least 3 components. Finally, a model employing complete cysteines and 2 additional neighboring atoms was used to reproduce the detailed structure of the PVDOS in the Fe−S stretch region. These results confirm the delocalization of the dynamic properties of the redox-active Fe site. Depending on the molecular model employed, the force constant $K_{Fe-S}$ for Fe−S stretching modes ranged from 1.24 to 1.32 mdyn/Å. $K_{Fe-S}$ is clearly diminished in reduced Rd; values from ∼0.89 to 1.00 mdyn/Å were derived from different models. In contrast, in the final models the force constants for S−Fe−S bending motion, $H_{S-Fe-S}$, were 0.18 mdyn/Å for oxidized Rd and 0.15 mdyn/Å for reduced Rd. The NRVS technique demonstrates great promise for the observation and quantitative interpretation of the dynamical properties of Fe−S proteins.

## Introduction

Rubredoxins are small (∼50 amino acid) electron-transfer proteins that contain a single $Fe(S\text{-}cys)_4$ redox center.[1] Apart from their role in specific biological catalytic reactions, rubredoxins serve as model systems for understanding the factors that determine reduction potentials in metalloproteins.[2,3] In this regard, investigators have systematically changed the central metal,[4,5] the primary coordination sphere ligands,[6] and more distant residues.[3,7] The relative importance of contributions to the redox properties from metal geometry, hydrogen-bonding, protein dipoles, water accessibility, and other factors are still being debated.

High-resolution X-ray crystal structures for oxidized *Desulfovibrio vulgaris* rubredoxin (*Dv* Rd) at 0.92 Å resolution (1RB9), *Pyrococcus furiosus* (*Pf*) Rd at 0.95 Å resolution (1BRF),[10] *Clostridium pasteurianum* (*Cp*) Rd at 1.1 Å (1IRO),[4]

[†] University of California.
[‡] Lawrence Berkeley National Laboratory.
[§] Stanford University.
[||] University of Georgia.
[⊥] Argonne National Laboratory.
[#] JASRI.

(1) Meyer, J.; Moulis, J.-M. Rubredoxin. In *Handbook of Metalloproteins*; Messerschmidt, A., Huber, R., Eds.; Wiley: New York, 2001; Vol. 1, pp 505−517.
(2) Niu, S.; Wang, X.-B.; Nichols, J. A.; Wang, L.-S.; Ichiye, T. *J. Phys. Chem. A* **2003**, *107*, 2898−2907.
(3) Ergenekan, C. E.; Thomas, D.; Fischer, J. T.; Tan, M. L.; Eidsness, M. K.; Kang, C.; Ichiye, T. *Biophys. J.* **2003**, *85*, 2818−2829.
(4) Dauter, Z.; Wilson, K. S.; Sieker, L. C.; Moulis, J. M.; Meyer, J. *Proc. Natl. Acad. Sci. U.S.A.* **1996**, *93*, 8836−8840.
(5) Maher, M.; Cross, M.; Wilce, M. C.; Guss, J. M.; Wedd, A. G. *Acta Crystallogr., D* **2004**, *60*, 298−303.
(6) Xiao, Z.; Lavery, M. J.; Ayhan, M.; Scrofani, S. D. B.; Wilce, M. C. J.; Guss, J. M.; Tregloan, P. A.; George, G. N.; Wedd, A. G. *J. Am. Chem. Soc.* **1998**, *120*, 4135−4150.


**10.1021/ja042960h CCC: $30.25** 

***Chart 1.*** (Left) "Pymol"[8] Representation of Oxidized *Pf* Rd, Including Sticks for Cysteine Residues, Illustrating Exposed Location of Fe Site (Red); (Right) "Crystalmaker"[9] Close-Up of Fe Site Showing Slight Compression of Fe−SCys8 and Fe−SCys41 Bonds and Distinction between ∼90° FeSCC Dihedral Angles for "Exposed" Cysteines and ∼180° FeSCC Dihedral Angles for "Buried" Cysteines (PDB Code 1BRF)[10]

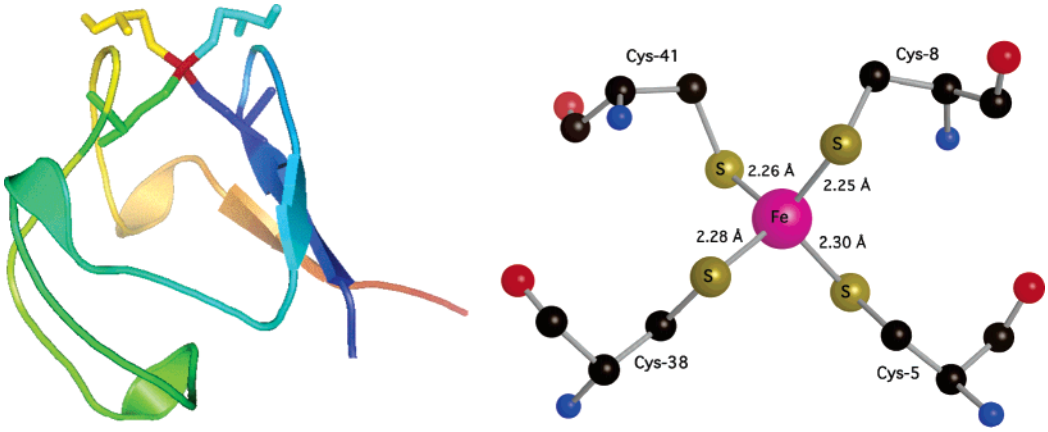


and *Pyrococcus abyssi* at 0.69 Å (1YK5),[11] as well as a *Pf* Rd neutron diffraction structure at 1.5 Å (1VCX)[12] all reveal a roughly tetrahedral $FeS_4$ site, often described as approaching $D_{2d}$ symmetry via a compression along an $S_4$ axis (Chart 1). In *Pf* Rd, this distortion results in two compressed (∼103 ± 1°) (Cys5S−Fe−SCys41 and Cys8S−Fe−SCys41) and four expanded (∼111°−114°) S−Fe−S angles; there are also two shorter Fe−S bond lengths (2.25−2.26 Å) (Fe−SCys8 and Fe−SCys41) and two slightly longer Fe−S bonds (2.28−2.30 Å) (Fe−SCys5 and Fe−SCys38). A similar pattern is seen in *Cp* Rd.[4] Upon reduction, an elongation of Fe−S bond lengths by an average of 0.096 Å (*Cp* Rd),[13] 0.033 Å (*Pf* Rd),[14] or 0.012 Å (L41A *Cp* Rd)[15,16] is found for reduced Rd. EXAFS studies have deduced typical average values for the Fe−S bond lengths as 2.29 Å in oxidized proteins and 2.34 Å in the reduced forms.[17]

The dynamical properties of the oxidized and reduced Fe sites play an important role in the redox properties of rubredoxins.[18] For oxidized Rd, the frequencies of bending and stretching modes are available from resonance Raman spectroscopy.[19−24] The strongest bands are near 315 $cm^{-1}$; these have been assigned to totally symmetric Fe−$S_4$ breathing modes. The splitting of the asymmetric Fe−S stretch region near 360 $cm^{-1}$ (degenerate $T_2$ modes in $T_d$ symmetry) into multiple bands demonstrates that the symmetry is lower than tetrahedral, and even the frequently used $D_{2d}$ symmetry is only approximate. (The structure of the reduced site has been described in terms of $C_2$ symmetry.[25]) With an $Fe(SCC)_4$ model, Spiro and co-workers used a Urey−Bradley force field to successfully reproduce most of the Fe−S stretching frequencies.[21−23] They emphasized the importance of ∼180° Fe−S−C−C dihedral angles for coupling Fe−S stretching with S−C−C bending and proposed that the Fe−S breathing mode frequency can be used as a diagnostic for the local conformation. In contrast, when Saito and co-workers employed a 423-atom Rd model, they found "no particular importance of these couplings".[24] They also observed additional modes at 397, ∼420, and ∼440 $cm^{-1}$ in the resonance Raman. The excitation profiles for bands near 130, 150, 174, and 184 $cm^{-1}$ have been reported;[22] these features have been assigned as a mixture of Fe−S−C and S−Fe−S bending modes[22] and HC−CH torsion.[23] Because of the loss of visible S→Fe charge-transfer bands when the protein is reduced, there are no published data about the vibrational modes for reduced Rd. Thus, even for this simplest of metalloproteins, there are serious gaps in our knowledge about the vibrational properties of the metal site.

Nuclear resonance vibrational spectroscopy (NRVS) is a relatively new technique with valuable characteristics for probing the dynamics of Fe in metalloproteins.[26,27] The NRVS experiment involves scanning an extremely monochromatic X-ray beam through a nuclear resonance. Apart from the familiar "zero phonon" (recoil-free) Mössbauer resonance, there are additional transitions that correspond to nuclear excitation in combination with excitation (Stokes) or de-excitation (anti-Stokes) of vibrational modes. The NRVS method offers less restrictive selection rules than infrared or resonance Raman spectroscopy; on resonance the only requirement for NRVS

(7) Kummerle, R.; Zhuang-Jackson, H.; Gaillard, J.; Moulis, J. M. *Biochemistry* **1997**, *36*, 15983−15991.
(8) DeLano, W. L. The PyMOL Molecular Graphics System; 2002.
(9) Palmer, D. *CrystalMaker*; CrystalMaker Software, Ltd.: Oxfordshire, OX5 1PF U.K., 2004; http://www.crystalmaker.co.uk.
(10) Bau, R.; Rees, D. C.; Kurtz, D. M.; Scott, R. A.; Huang, H. S.; Adams, M. W. W.; Eidsness, M. K. *J. Biol. Inorg. Chem.* **1998**, *3*, 484−493.
(11) Bonisch, H.; Schmidt, C. L. *Acta Crystallogr., D* **2005**, *61*, 990−1004.
(12) Kurihara, K.; Tanaka, I.; Chatake, T.; Adams, M. W. W.; Jenney, F. E., Jr.; Moiseeva, N.; Bau, R.; Niimura, N. *Proc. Natl. Acad. Sci. U.S.A.* **2004**, *101*, 11215−11220.
(13) Min, T.; Ergenkan, C. E.; Eidsness, M. K.; Ichiye, T.; Kang, C. *Protein Sci.* **2004**, *10*, 613−621.
(14) Day, M. W.; Hsu, B. T.; Joshua-Tor, L.; Park, J. B.; Zhou, Z. H.; Adams, M. W. W.; Rees, D. C. *Protein Sci.* **1992**, *1*, 1494−1507.
(15) Park, I. Y.; Youn, B.; Harley, J. L.; Eidsness, M. K.; Smith, E.; Ichiye, T.; Kang, C.-H. *J. Biol. Inorg. Chem.* **2004**, *9*, 423−428.
(16) The anomalously small value in the latter study might reflect photoreduction of the 'oxidized' structure.
(17) George, G. N.; Pickering, I. J.; Prince, R. C.; Zhou, Z. H.; Adams, M. W. W. *J. Biol. Inorg. Chem.* **1996**, *1*, 226−230.
(18) May, V.; Kühn, O. *Charge and Energy Transfer Dynamics in Molecular Systems*, 2nd ed.; Wiley: New York, 2004.
(19) Long, T. V.; Loehr, T. M. *J. Am. Chem. Soc.* **1970**, *92*, 6384−6386.
(20) Long, T. V.; Loehr, T. M.; Allkins, J. R.; Lovenberg, J. *J. Am. Chem. Soc.* **1971**, *93*, 1809−1811.
(21) Yachandra, V. K.; Hare, J.; Moura, I.; Spiro, T. G. *J. Am. Chem. Soc.* **1983**, *105*, 6455−6461.
(22) Czernuszewicz, R. S.; LeGall, J.; Moura, I.; Spiro, T. G. *Inorg. Chem.* **1986**, *26*, 696−700.
(23) Czernuszewicz, R. S.; Kilpatrick, L. K.; Koch, S. A.; Spiro, T. G. *J. Am. Chem. Soc.* **1994**, *116*, 1134−1141.
(24) Saito, H.; Imai, T.; Wakita, K.; Urushiyama, A.; Yagi, T. *Bull. Chem. Soc. Jpn.* **1991**, *64*, 829−836.
(25) Vrajmasu, V. V.; Bominaar, E. L.; Meyer, J.; Münck, E. *Inorg. Chem.* **2002**, *41*, 6358−6371.
(26) Alp, E.; Sturhahn, W.; Toellner, T. S.; Zhao, J.; Hu, M.; Brown, D. E. *Hyperfine Interact.* **2002**, *144/145*, 3−20.
(27) Sturhahn, W. *J. Phys.: Condens. Matter* **2004**, *16*, S497−S530.

intensity in a given normal mode is motion of the resonant nucleus $j$ (in our case $^{57}$Fe) along the direction of the incident X-ray beam. The details of NRVS theory have been explained elsewhere;[27,28] the bottom line for the current study is that a phonon NRVS transition for normal mode α contributes an area $\phi$ to the normalized excitation probability $S(\bar{\nu})$ that is directly proportional to the Fe mode composition factor $e_{j\alpha}{}^2$ and inversely proportional to $\bar{\nu}_\alpha$:[28,29]

$$\phi_\alpha = \frac{1}{3}\frac{\bar{\nu}_R}{\bar{\nu}_\alpha} e_{j\alpha}{}^2(\bar{n}_\alpha + 1)f \qquad (1)$$

In the above equation, $\bar{\nu}_\alpha$ is the difference between the photon energy and the recoil-free nuclear resonance energy in wavenumbers, $\bar{\nu}_R$ is the recoil energy $\bar{\nu}_R = \hbar^2k^2/2m_{Fe}$ or ~16 cm$^{-1}$, $\bar{n}_\alpha = [\exp(hc\bar{\nu}_\alpha/k_BT) - 1]^{-1}$ is the thermal occupation factor for a mode of frequency $\bar{\nu}_\alpha$ at temperature $T$,[28] and the recoilless fraction $f$ depends on $\langle x_{Fe}{}^2\rangle$, the mean square fluctuation of the Fe nucleus along the beam direction, via $f = \exp(-k^2\langle x_{Fe}{}^2\rangle)$. For randomly oriented protein samples where it is difficult to observe discrete NRVS transitions, it is useful to define an $^{57}$Fe-centered partial vibrational density of states (PVDOS), $D_{Fe}(\bar{\nu})$, using a line shape function $L(\bar{\nu} - \bar{\nu}_\alpha)$:[28,30]

$$D_{Fe}(\bar{\nu}) = \sum_\alpha e_{Fe,\alpha}^2 L(\bar{\nu} - \bar{\nu}_\alpha) \qquad (2)$$

The $^{57}$Fe PVDOS can be extracted from the raw NRVS using the PHOENIX software package,[31] and the Fe mode composition factor $e_{Fe,\alpha}{}^2$ for a given eigenvector α can be calculated from a normal mode analysis via:[28,32]

$$e_{Fe,\alpha}{}^2 = \frac{m_{Fe}r_{Fe,\alpha}{}^2}{\sum_j m_j r_{j\alpha}{}^2} \qquad (3)$$

where $m_j$ and $r_{j\alpha}{}^2$ are the mass of atom $j$ and its mean square motion, respectively.

In this paper we report the $^{57}$Fe NRVS for *Pf* Rd in both oxidized and reduced forms. Resonance Raman spectra for oxidized Rd are also presented. Normal mode calculations on models of gradually increasing complexity are used to reproduce and interpret the experimental data. The NRVS data contain information about both the frequency and the amplitude of Fe motion, they extend to lower frequencies than typical metalloprotein resonance Raman spectra, and they reveal midrange modes not evident in the Raman data. By combining NRVS and Raman spectra, we were able to refine a Urey−Bradley force field for the oxidized site. We could also (for the first time) observe vibrational modes for the reduced site, and we refined a force field for this form as well. The results are compared with previous Raman and molecular mechanics analyses of rubredoxins.

## Experimental Section

**Protein Purification and Sample Preparation.** *Pf* met-Rd (recombinant rubredoxin still containing the unprocessed N-terminal methionine residue) was purified by published procedures.[33] Reconstitution of rubredoxin with various transition metals is now routine,[34] and the zinc-containing protein has been shown to refold normally by NMR.[35] The protein was precipitated in 20% trichloroacetic acid/200 mM β-mercaptoethanol to remove the native iron. The protein (100 mg) was dissolved in degassed 0.5 M Tris acetate pH 8/200 mM β-mercaptoethanol to a final concentration of 1 mM in a sealed serum vial. A 5-fold molar excess of powdered $^{57}$Fe (from Oak Ridge National Laboratories, 4.8 mg) was dissolved in 200 μL of *aqua regia* and added to the denatured protein. This mixture was stirred anaerobically overnight at 25 °C. Extensive washing by ultrafiltration yielded 90 mg of $^{57}$Fe-metRd in a deep red solution (22 mM in 50 mM Tris acetate pH 8.0) that was flash-frozen in liquid nitrogen. Reconstitution with $^{57}$Fe gave UV/visible spectra indistinguishable from wild-type protein. A reduced sample was prepared by dithionite reduction in an anaerobic $N_2$-containing glovebox with an $O_2$ concentration <0.1 ppm. For NRVS measurements, the protein samples were loaded into 3 by 7 by 1 mm$^3$ (interior dimensions) Lucite cuvettes.

**Nuclear Resonance Vibrational Spectroscopy.** $^{57}$Fe NRVS spectra were recorded using published procedures[27] on multiple occasions at beamline 3-ID at the Advanced Photon Source (APS)[36] and BL09XU at SPring-8, Japan.[37] Beamline 3-ID provided ~2.5 × 10$^9$ photons/s in 1 meV bandwidth at 14.4125 keV in a 1 mm (vertical) × 3 mm (horizontal) spot. The monochromators consisted of a water-cooled diamond (1,1,1) double crystal monochromator with a 1.1 eV bandpass, followed by two separate Si channel-cut crystals, mounted on high precision rotation stages (Kohzu KTG-15AP) in a symmetric geometry. The first channel-cut crystal uses two Si(4,0,0) reflections; the second uses two reflections at the highest order possible (10,6,4) at 14.4125 keV. The flux at Spring-8 was ~4 × 10$^9$ in a 3.5 meV bandwidth; the monochromators there consisted of a water-cooled Si-(1,1,1) double crystal monochromator and asymmetrically cut (5,1,1) and (9,7,5) crystals. During all NRVS measurements, the samples were maintained at low temperatures using liquid He (APS) or liquid $N_2$ (SPring-8) cryostats. Since the temperature sensors were not directly in contact with the samples, temperatures for individual spectra were calculated using the ratio of anti-Stokes to Stokes intensity according to: $S(-E) = S(E)\exp(-E/kT)$. Spectra were recorded between −20 and 80 meV in steps of 0.25 meV. Delayed nuclear fluorescence and Fe K fluorescence (from internal conversion) were recorded with a single avalanche 1 cm$^2$ square photodiode (APD) at the APS and with an APD array at Spring-8.[38] Each scan took about 40 min, and all scans were added and normalized to the intensity of the incident beam.

**Raman Spectroscopy.** Resonance Raman spectra were recorded in a backscattering geometry from a rubredoxin solution immersed in a Suprasil liquid nitrogen Dewar at 77K. The excitation source was a Coherent Innova-2 $Ar^+/Kr^+$ laser operated at 488, 514.5, 568, and 647 nm, using a moderate cw laser power of 25−35 mW. No sample radiation damage was observed. The spectra were recorded with a Spex model 1877 triple Raman spectrometer, using a cooled Spectrum One 594 CCD detector. Each spectrum corresponds to data from about 8−16

(28) Leu, B. M.; Zgierski, M. Z.; Wyllie, G. R. A.; Scheidt, W. R.; Sturhahn, W.; Alp, E. E.; Durbin, S. M.; Sage, J. T. *J. Am. Chem. Soc.* **2004**, *126*, 4211−4227.
(29) Sturhahn, W.; Toellner, T. S.; Alp, E. E.; Zhang, X.; Ando, M.; Yoda, Y.; Kikuta, S.; Seto, M.; Kimball, C. W.; Dabrowski, B. *Phys. Rev. Lett.* **1995**, *74*, 3832−3835.
(30) Sage, J. T.; Paxson, C.; Wyllie, G. R. A.; Sturhahn, W.; Durbin, S. M.; Champion, P. M.; Alp, E. E.; Scheidt, W. R. *J. Phys.: Condens. Matter* **2001**, *13*, 7707−7722.
(31) Sturhahn, W. *Hyperfine Interact.* **2000**, *125*, 149−172.
(32) Chumakov, A. I.; Rüffer, R.; Leupold, O.; Sergueev, I. *Struct. Chem.* **2003**, *14*, 109−119.
(33) Jenney, F. E., Jr.; Adams, M. W. W. *Methods Enzymol.* **2001**, *334*, 45−55.
(34) Moura, I.; Teixeira, M.; LeGall, J.; Moura, J. J. *J. Inorg. Biochem.* **1991**, *44*, 127−139.
(35) Blake, P. R.; Park, J. B.; Bryant, F. O.; Aono, S.; Magnuson, J. K.; Eccleston, E.; Howard, J. B.; Summers, M. F.; Adams, M. W. *Biochemistry* **1991**, *30*, 10885−10895.
(36) Toellner, T. *Hyperfine Interact.* **2000**, *125*, 3−28.
(37) Yoda, Y.; Yabashi, M.; Izumi, K.; Zhang, X. W.; Kishimoto, S.; Kitao, S.; Seto, M.; Mitsui, T.; Harami, T.; Imai, Y.; Kikuta, S. *Nucl. Instrum. Methods Phys. Res, Sect. A* **2001**, *467*, 715−718.

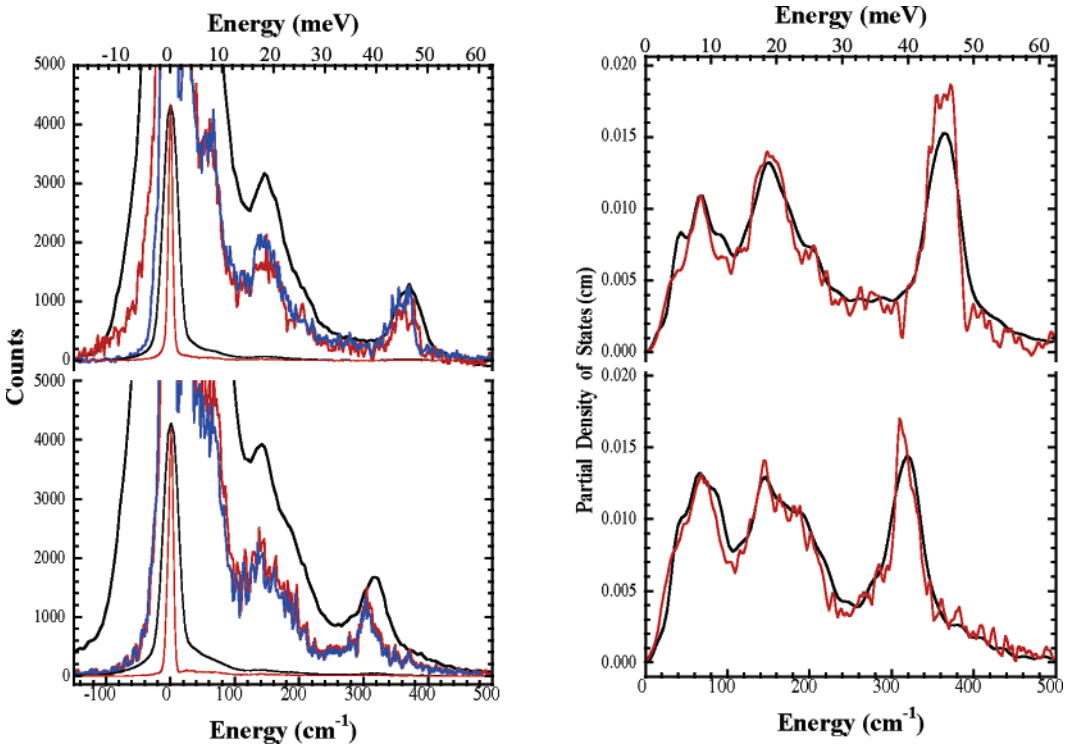


***Figure 1.*** Left, top: raw NRVS spectra for oxidized *Pf* Rd taken at SPring-8 at 78 K (black) and on separate occasions at the APS at 60 K (blue) and 35 K (red). Left, bottom: NRVS for reduced *Pf* Rd taken at SPring-8 at 78 K (black) and on separate occasions at the APS at 35 K (blue) and 150 K (red). Right, top: Extracted Fe partial vibrational density of state functions, $D_{Fe}(\bar{\nu})$, for oxidized *Pf* Rd taken at SPring-8 (black) and weighted average of APS data (red). Bottom, left: $D_{Fe}(\bar{\nu})$ for reduced *Pf* Rd taken at SPring-8 (black) and weighted average of APS data (red). SPring-8 data were calibrated to APS energy scale.

h of measurement. The Raman spectra were calibrated using peaks at 218 and 314 $cm^{-1}$ in a room-temperature $CCl_4$ sample. The entrance slit and slits 2/3 were set to 0.1 mm, yielding ~3 $cm^{-1}$ frequency resolution.

**Normal Mode Calculations.** The normal mode calculations were carried out on different structural models derived from the crystallographic coordinates and assembled with the program "Atoms" from Shape Software.[39] A modification of program "Vibratz" was used to calculate the normal modes and NRVS spectra,[39,40] using the Wilson's GF matrix method and a Urey−Bradley force field. A QR algorithm was used for finding eigenvectors.[41] In principle, a normal mode analysis yields the NRVS intensity on an absolute basis, without adjustable scale factors.[28] However, for presentation purposes, scale factors were sometimes used to adjust the maximum value of the simulated spectrum with the peak in the experimental PVDOS; these values are provided in the text.

**Density Functional Theory Calculations.** Geometry optimized DFT calculations on $[FeCl_4]^{-/2-}$ and $[Fe(SMe)_4]^{-/2-}$ were done in ADF 2004 software using BP86 GGA functional[42,43] and the TZP (triple-ζ) basis set. The bond dissociation energy was calculated from the difference of fully optimized complex and fully optimized charged fragments. The $A_1$ stretching mode simulation was done with the "Lineartransit" keyword in the ADF program and with full optimization at each point. Frequencies were calculated on these optimized structures in the Gaussian 03 package using the same functional and the 6-311g* basis set.

## Results

**NRVS Spectra.** The raw NRVS spectra for oxidized and reduced *Pf* rubredoxin are presented in Figure 1. Preliminary results for the oxidized sample have been previously reported.[44] On one hand, the SPring-8 spectra are broader than the APS spectra, thanks to the lower monochromator resolution (3.5 meV vs 1 meV).[45] On the other hand, the statistics for the SPring-8 spectra are better, thanks to the greater number of NRVS events collected (due to higher incident flux and larger collection solid angle). Three bands, near 70, 150, and 360 $cm^{-1}$, are observed (as distinct peaks or shoulders) in oxidized spectra from both SPring-8 and APS. In the spectra for the reduced protein, the highest frequency band shifts down to 303 $cm^{-1}$, while the broad features near 70 and 150 $cm^{-1}$ move relatively little.

Although the raw spectra appear rather different, after subtraction of the elastic component and conversion to density of states spectra (Figure 1), the resultant $D_{Fe}(\bar{\nu})$ curves agree reasonably well (apart from resolution differences). This lends confidence to the significance of moderate intensity between the main peaks, as discussed below. It also underscores the significance of the features between 20 and 100 $cm^{-1}$; they are not artifacts of the background subtraction process (see Supporting Information).

In both reduced and oxidized spectra, the highest frequency modes have the greatest amplitude and hence the largest fractional contribution of Fe kinetic energy.[26] In $T_d$ symmetry,

(38) Kishimoto, S.; Yoda, Y.; Seto, M.; Kitao, S.; Kobayashi, Y.; Haruki, R.; Harami, T. *Nucl. Instrum. Methods Phys. Res, Sect. A* **2004**, *513*, 193−196.
(39) Shape Software, http://www.shapesoftware.com/.
(40) Dowty, E. *Phys. Chem. Miner.* **1987**, *14*, 67−79.
(41) Engeln-Mueller, G.; Uhlig, F. *Numerical Algorithms with C*; Springer-Verlag: 1996.
(42) Becke, A. D. *Phys. Rev. A* **1988**, *38*, 3098−3100.
(43) Perdew, J. P. *Phys. Rev. B* **1986**, *33*, 8822−8824.
(44) Bergmann, U.; Sturhahn, W.; Linn, D. E.; Jenney, F. E., Jr.; Adams, M. W. W.; Rupnik, K.; Hales, B. J.; Alp, E. E.; Mayse, A.; Cramer, S. P. *J. Am. Chem. Soc.* **2003**, *125*, 4016−4017.
(45) In more recent experiments, the SPring-8 beamline has achieved ~1.1 meV resolution.

these features would be assigned to $T_2$ modes, since Fe motion is excluded by symmetry for the $A_1$ and E modes. By comparison with previous resonance Raman work, we already know that the oxidized band centered near 360 $cm^{-1}$ corresponds to asymmetric Fe−S stretching motion. The ∼303 $cm^{-1}$ band in the reduced protein spectrum is the same type of asymmetric Fe−S stretching motion, observed here for the first time.

For the oxidized protein, although the center of gravity for the Fe−S stretch region is at ∼360 $cm^{-1}$, there is significant intensity in an envelope between 345 and 375 $cm^{-1}$. With the improved resolution of the APS spectra, we can conclude that the width of these broad bands is not an experimental artifact; rather, it derives from the lower symmetry and/or extensive vibrational coupling of the Fe in a protein environment. The important point is that the asymmetric stretching region for oxidized *Pf* Rd has a fwhm that is nearly 4 times the experimental resolution. The 303 $cm^{-1}$ band in the reduced *Pf* Rd spectrum also has significant broadening beyond the experimental resolution.

The broad intensity in both spectra between 100 and 200 $cm^{-1}$ derives primarily from S−Fe−S and Fe−S−C bending motion. Here, the oxidized spectrum has a peak near 150 $cm^{-1}$, a resolved sideband at 120 $cm^{-1}$, a shoulder at ∼175 $cm^{-1}$, and an additional structure near 200 $cm^{-1}$. For the reduced protein spectrum, this region can be interpreted as split into components at 117, 143, 163, 180, and ∼200 $cm^{-1}$. The width of these features in both spectra shows that they represent a number of unresolved components. In the original Raman work by Long and co-workers,[20] bending modes were reported at 126 and 150 $cm^{-1}$ and, respectively, assigned as E and $T_2$ modes in $T_d$ symmetry. A study by Yachandra et al. observed shoulders only at 126 and 177 $cm^{-1}$ with 4825 Å excitation,[21] although they did see peaks from S−Fe−S bending at 155 and 157 $cm^{-1}$ in Fe−S model complexes. Later, Czernuszewicz and co-workers studied the excitation frequency dependence of the bend region and found a feature at ∼130 $cm^{-1}$ enhanced with 4965 Å excitation, while a ∼150 $cm^{-1}$ peak became strong when probed with 5682 Å radiation.[22] By reference to this work, we can assign the main NRVS intensity in the ∼150 $cm^{-1}$ region to motion derived from the asymmetric $T_2$ bend motion of $T_d$ symmetry, which is NRVS-allowed. The weaker intensity at ∼125 $cm^{-1}$ derives from doubly degenerate E modes, which are NRVS-forbidden in $T_d$ symmetry, but become allowed thanks to the lower symmetry of the protein $FeS_4$ site and mixing with cysteine side chain motions.

Reproducible NRVS features are also seen below 100 $cm^{-1}$; this is outside the range of typical protein resonance Raman data. With the oxidized form, the low-frequency region seems to have at least one component near 70 $cm^{-1}$ and another near 40 $cm^{-1}$; the spectrum of the reduced form is similar but broader in this region.

**Resonance Raman Spectra.** The resonance Raman spectrum for *Pf* Rd has not been reported. For comparison with the NRVS, we recorded Raman spectra using several different excitation wavelengths (Figure 2). In sharp contrast with the NRVS, the strongest Raman band is near 313 $cm^{-1}$; in $T_d$ symmetry this would be the totally symmetric Fe−S stretching mode. Similar bands at 312−314 $cm^{-1}$ have been reported for rubredoxins from *D. gigas*, *D. desulfuricans*, and *M. elsdenii*.[21−23] With 568 nm excitation, we resolve a peak at 323 $cm^{-1}$ that was seen as a shoulder in previous work,[22] and a band at ∼332 $cm^{-1}$ becomes more apparent.

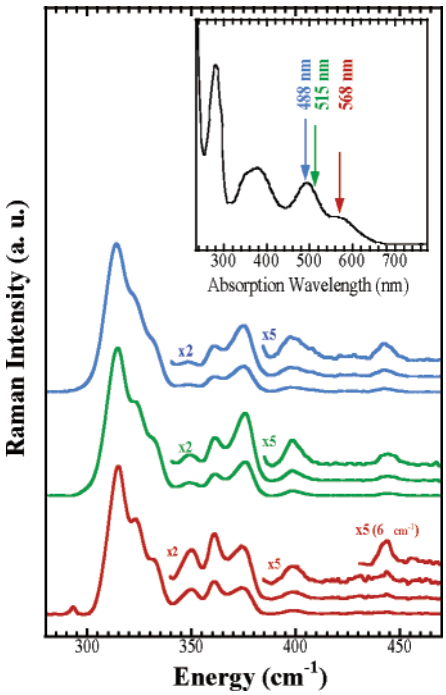


***Figure 2.*** Resonance Raman spectra for oxidized *Pf* Rd, using excitation at 488 nm (blue), 515 nm (green), and 568 nm (red). Inset: visible absorption spectrum for oxidized *Pf* Rd.

The strongest remaining Fe−S stretching modes are seen in the resonance Raman spectrum at higher frequencies (Figure 2). Two components can be distinguished at ∼347 and ∼375 $cm^{-1}$; an intermediate peak at ∼360 $cm^{-1}$ is clearest with 568 nm excitation. Each of these bands, which are derived from the $T_2$ $\nu_3$ modes in $T_d$ symmetry, might contain additional unresolved structure. Even in simple model complexes such as $[Fe(SCH_3)_4]^-$, Spiro's group observed that the $\nu_{3c}$ mode was split by Fermi resonance with an Fe−S−C bending mode overtone.[23] At higher frequencies, we see modes at ∼395 and 440 $cm^{-1}$ which correspond to similar features observed by Saito and co-workers.[24]

**Normal Mode Analysis.** To quantitatively interpret the NRVS spectra and to set the stage for analysis of seemingly more complex problems such as hydrogenase and nitrogenase, we undertook a normal mode analysis using a Urey−Bradley force field. The resonance Raman spectra of rubredoxin and $[Fe(SR)_4]^{n-}$ model complexes have been extensively analyzed by this approach, and our interpretation relies on much of this body of work.[21−23] The Cartesian coordinates for the Fe ligands of reduced wild-type and oxidized met-rubredoxin were taken from the X-ray crystal structures (1CAD and 1BQ8, respectively).[10,14] We began with a simple tetrahedral $FeS_4$ model (not shown). As expected, this can reproduce the central positions of the S−Fe−S bend and stretch regions (the 2 distinct $T_2$ modes), but lower symmetry is necessary to explain the splitting of these bands, and additional atoms are needed to reproduce the lower energy features.

***$D_{2d}$* Fe(SC)$_4$ Model.** We next explored the simplest $Fe(SC)_4$ models that could explain the splitting of the higher frequency modes as well as the appearance of the NRVS spectra below 100 $cm^{-1}$. We began with a $D_{2d}$ $Fe(SC)_4$ model similar to those

***Table 1.*** Comparison of Force Constants Used in Simulations on Oxidized and Reduced *Pf* Rd vs Values Employed by (Cz) Czernuszewicz et al.[23] and (Sa) Saito et al.[24]

| | | | | | |
|---|---|---|---|---|---|
| **K (Fe-S) (oxidized)** | 1.32 (a)<br>1.26 (b)<br>1.24 (c)<br>1.27 (Cz)<br>1.36 (Sa) | **H (S-Fe-S) (ox)** | 0.16 (a)<br>0.21 (b)<br>0.18 (c)<br>0.35 (Cz)<br>0.43 (Sa) | ***f* (FeS-FeS) (ox)** | 0.07 (a)<br>0.02 (b)<br>0.02(c)<br>0.07 (Cz) |
| **K (Fe-S) (reduced)** | 1.00 (a)<br>0.89 (b)<br>0.92(c) | **H (S-Fe-S) (red)** | 0.12 (a)<br>0.16 (b)<br>0.15 (c) | ***f* (FeS-FeS) (red)** | 0.07 (a)<br>0.02 (b)<br>0.01(c) |
| **K (S-C) (ox/red)** | 3.05 (a-c)<br>3.05 (Cz)<br>2.00 (Sa) | **H (S-C-C) (ox/red)** | 0.16 (b)<br>0.82(c)<br>0.82 (Cz)<br>0.42 (Sa) | **F (S···S) (ox/red)** | 0.12 (a)<br>0.14 (b)<br>0.066 (c)<br>0.0335 (Cz) |
| **K (C-C) (ox/red)** | 4.8 (a-c)<br>4.8 (Cz)<br>3.7 (Sa) | **H (S-C-H) (ox/red)** | 0.62 (c)<br>0.62 (Cz) | **F (Fe···C) (ox)** | 0.08 (b)<br>0.011 (c)<br>0.12 (Cz) |
| **K (C-H) (ox/red)** | 4.7 (c)<br>4.7 (Cz) | **H (H-C-H) (ox/red)** | 0.54 (c)<br>0.54 (Cz) | **F (Fe···C) (red)** | 0.06 (c) |
| **K (C-N) (ox/red)** | 5.2 (c)<br>4.2 (Sa) | **H (C-C-H) (ox/red)** | 0.26(c)<br>0.54 (Cz) | **t(SFe-SC) (ox)** | 0.036 (a)<br>0.02 (b) |
| **K (C=O) (ox/red)** | 8.6 (c)<br>9.0 (Sa) | **H (C-C-C) (ox/red)** | 0.31 (c)<br>0.45 (Sa) | **t(SFe-SC) (red)** | 0.036 (a)<br>0.08 (b) |
| **K (N-H) (ox/red)** | 6.1 (c) | **H (C-C-N) (ox)** | 0.2 (c)<br>0.4 (Sa) | **t(FeS-CC)[d] (ox)** | 0.25 (b) |
| | | | | **t(FeS-CC)[d] (red)** | 0.26 (b) |
| **H (Fe-S-C) (ox)** | 0.17 (a)<br>0.18 (b)<br>0.3(c)<br>0.25 (Cz)<br>0.62 (Sa) | **H (C-C-N) (red)** | 0.3 (c) | **t(FeS-CC)[e] (ox/red)** | 0.05 (b) |
| | | | | **t(CC-NC) (ox/red)** | 0.001(c) |
| **H (Fe-S-C) (ox/red)** | 0.17 (a)<br>0.18 (b)<br>0.2(c) | **H (C-N-C) (ox/red)** | 0.2(c)<br>0.42 (Sa) | **t(HC-CH) (ox/red)** | 0.0216 (c)<br>0.0216 (Cz) |
| | | **H (C-N-C) (red)** | 0.32 (c) | **t(CC-NH) (ox/red)** | 0.007(c) |
| **H (C-N-H) (ox/red)** | 0.26 (c) | **H (C-N-C) (red)** | 0.32 (c) | ***f* (SC-SCC) (ox/red)** | 0.35 (c)<br>0.35 (Cz) |
| **H (N-C-H) (ox)** | 0.23 (c) | **t(HC-NH) (ox/red)** | 0.001 (c) | ***f* (CC-SCC) (ox/red)** | 0.35 (c)<br>0.35 (Cz) |
| **H (N-C-H) (red)** | 0.33 (c) | **t(OC-NC) (ox/red)** | 0.015 (c) | ***f*(FeSC/SCH) (ox/red)** | 0.22 (c)<br>0.22 (Cz) |

[a] Model $D_{2d}$ $Fe(SC)_4$. [b] Model $C_1$ $Fe(SCC)_4$. [c] Model $Fe(S\text{-}cysX_5)_4$. [d] FeS−CC dihedral angle is 90°. [e] FeS−CC dihedral angle is 180°; units for force constants: K = stretching (mdyn/Å), H = bending (mdyn Å/rad$^2$), F = nonbonded interaction (mdyn/Å), f = stretch−stretch and stretch−bend interaction (mdyn/rad), t = torsional bend (mdyn/Å).

used by Spiro and co-workers.[22] Starting from published values, the Urey−Bradley force field parameters were adjusted to match the main peaks in the experimental $D_{Fe}(\bar{\nu})$ spectrum. The resulting parameters are listed in Table 1, the calculated frequencies and potential energy distribution (PED) for each normal mode are provided in Table S1 and Table S2 for oxidized and reduced Rd, respectively, and comparisons between experimental and calculated $D_{Fe}(\bar{\nu})$ are shown in Figure 3.

The $D_{2d}$ $Fe(SC)_4$ model yields six discrete frequencies, and it explains the three main regions of the spectrum as primarily Fe−S stretch, S−Fe−S bend, and Fe−S−C bend. The additional carbons yield a pair of new modes at 67 and 85 cm$^{-1}$; the potential energy of which derives from a mixture of S−Fe−S and Fe−S−C bending or mostly SFe−SC torsion respectively (Table S1). This model predicts that the degenerate $\nu_3$ mode in $T_d$ symmetry is split into E + $B_2$ modes; the best simulation for oxidized Rd yielded peaks at 348 and 366 cm$^{-1}$, as opposed to the three asymmetric stretch bands seen by resonance Raman. The $D_{2d}$ model also predicts a totally symmetric breathing mode that is NRVS forbidden, but there is in fact some intensity in the 315−330 cm$^{-1}$ region. The $D_{2d}$ $Fe(SC)_4$ model clearly has higher symmetry than evidenced by the experimental data.

***$C_1$* Fe(SCC)$_4$ Model.** We next lowered the symmetry to $C_1$ and added the cysteine Cα carbon atoms, putting all atoms at the oxidized or reduced Rd crystal structure coordinates; for brevity we refer to these as $Fe(SCC)_4$ models. Additional features of the PVDOS are reproduced with these models (Figure 3). For oxidized Rd, the $T_2$ band in the calculations splits into components at 348, 354, and 372 cm$^{-1}$, consistent with the NRVS envelope between 345 and 380 cm$^{-1}$, as well as the observed Raman frequencies. This model also produces three additional pairs of eigenvectors near 170, 190, and 255 cm$^{-1}$; these modes begin to fill in the PVDOS between the main peaks at 150 and 360 cm$^{-1}$.

A scale reduction factor of 1.86 (1.96) was required to match the peak intensity of the calculated PVDOS with the experimentally derived curve for oxidized (reduced) Rd. As a reminder, the PHOENIX program sets the integrated PVDOS

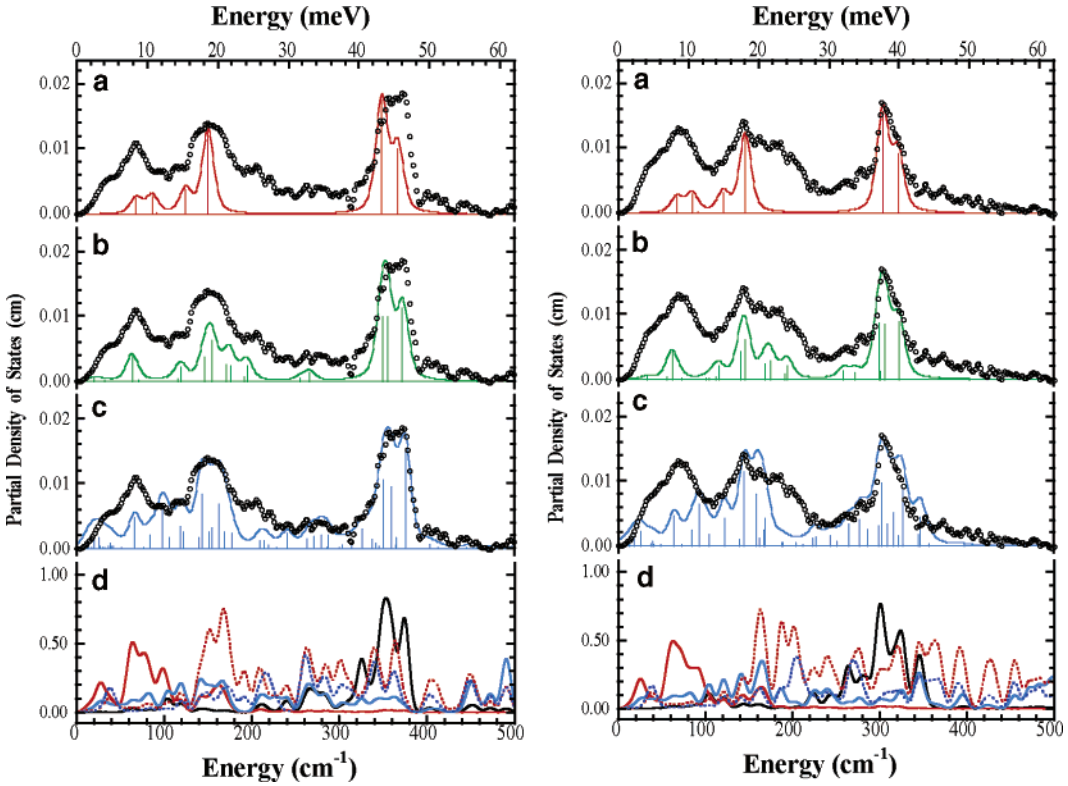


***Figure 3.*** Left panel: oxidized *Pf* Rd. Right panel: reduced *Pf* Rd. (Top to bottom for each panel) (a) $^{57}$Fe PVDOS (○) and simulation (red solid line) for $Fe(SC)_4$ model in $D_{2d}$ symmetry. Sticks represent intensities of individual normal modes. (b) $^{57}$Fe PVDOS (○) and simulation (green solid line) for $Fe(SCC)_4$ model using crystallographic coordinates. (c) $^{57}$Fe PVDOS (○) and simulation (blue solid line) using $Fe(ScysX_5)_4$ model. (d) PED for $Fe(ScysX_5)_4$ models. Curves represent contributions from Fe−S stretching (black solid line), S−Fe−S (red solid line), S−C−C (blue solid line), C−C−N (red dashed line), and C−C−C (blue dashed line) bending. In all cases, the calculated PVDOS has been broadened with an approximate Voigt profile (50% Gaussian, 50% Lorentzian, 8 $cm^{-1}$ fwhm) to account for experimental and natural line widths.

to a value of 3, in accord with the normalization condition for $D_{Fe}(\bar{\nu})$.[30] Apart from a small acoustic mode contribution, the VIBRATZ routine will also yield an integrated PVDOS of ~3, with 1 unit each for *x*, *y*, and *z* directions. The need to reduce the calculated peak intensity in the asymmetric Fe−S stretch region indicates that Fe contributes less to the kinetic energy of these modes than predicted by the simple model. To conserve integrated intensity, there must be additional modes where $^{57}$Fe contributes to the kinetic energy; the result is a broader spectrum with the same area but less intense peaks.

**$Fe(S\text{-}cysX_5)_4$ Model.** To allow for additional normal modes, we added all the remaining cysteine atoms to the model, as well as the carbonyl C and O of the residue adjacent to the cysteine N, and the amide N of the residue bound to the cysteine carbonyl. Initial values for the force constants associated with these peripheral atoms were obtained from the "TINKER" molecular modeling software.[46] Several reports have commented on unreasonably large motions in bending modes for atoms that terminate small molecular models of protein metal sites;[23,47,48] we found this in some of our simulations as well. To reduce these motions on the atoms of interest, a final atom with mass 12 was added to each end. In the course of revising this manuscript, we discovered that a more sophisticated approach was employed by Qiu and co-workers in their "chromophore in protein" calculations.[49] They included all of the protein atoms in their model for plastocyanin but assigned masses of 999 to polypeptide atoms more than six atoms away (via the ligating side chain) from the central Cu.

The force constants for the core atoms were then refined, with respect to both oxidized and reduced PVDOS (Table 1). The resultant $K_{Fe-S}$ for the oxidized protein was 1.24 mdyne $Å^{-1}$, essentially the same as the 1.27 mdyne $Å^{-1}$ used by Czernuszewicz et al.[23] or the 1.36 mdyne $Å^{-1}$ value used by Saito and co-workers.[24] $H_{SFeS}$ was 0.16 mdyne-Å, smaller than the 0.35 or 0.43 mdyne $Å^{-1}$ values used by Czernuszewicz[23] or Saito.[24] Both of these groups were much less concerned with the bending mode region of the spectrum. As shown in Figure 3, the $Fe(S\text{-}cysX_5)_4$ model does a much better job of simulating the asymmetric Fe−S stretch region, and it also continues the trend of filling in intensity between 150 and 360 $cm^{-1}$ and below 100 $cm^{-1}$. The scale factor of 1.03 indicates that a model of this size is a reasonable description of the normal modes that contain most of the Fe kinetic energy. The largest remaining discrepancies are below 100 $cm^{-1}$; a much larger model is needed to realistically describe the large-scale protein motions in this region.

With the oxidized $Fe(S\text{-}cysX_5)_4$ model, in the asymmetric Fe−S stretch region the three strongest NRVS components are at 375, 358, and 350 $cm^{-1}$ (Figure 3). Of all the modes derived from the normal mode analysis, these have the purest composition; they are about 50% Fe−S stretch (Table S1 and Figure

(46) Tinker - Software Tools for Molecular Design, http://dasher.wustl.edu/tinker/.

(47) Qiu, D.; Kilpatrick, L.; Kitajima, N.; Spiro, T. G. *J. Am. Chem. Soc.* **1994**, *116*, 2585−2590.
(48) Urushiyama, A.; Tobari, J. *Bull. Chem. Soc. Jpn.* **1990**, *63*, 1563−1571.
(49) Qiu, D.; Dasgupta, S.; Kozlowski, P. M.; Goddard, W. A.; Spiro, T. G. *J. Am. Chem. Soc.* **1998**, *120*, 12791−12797.

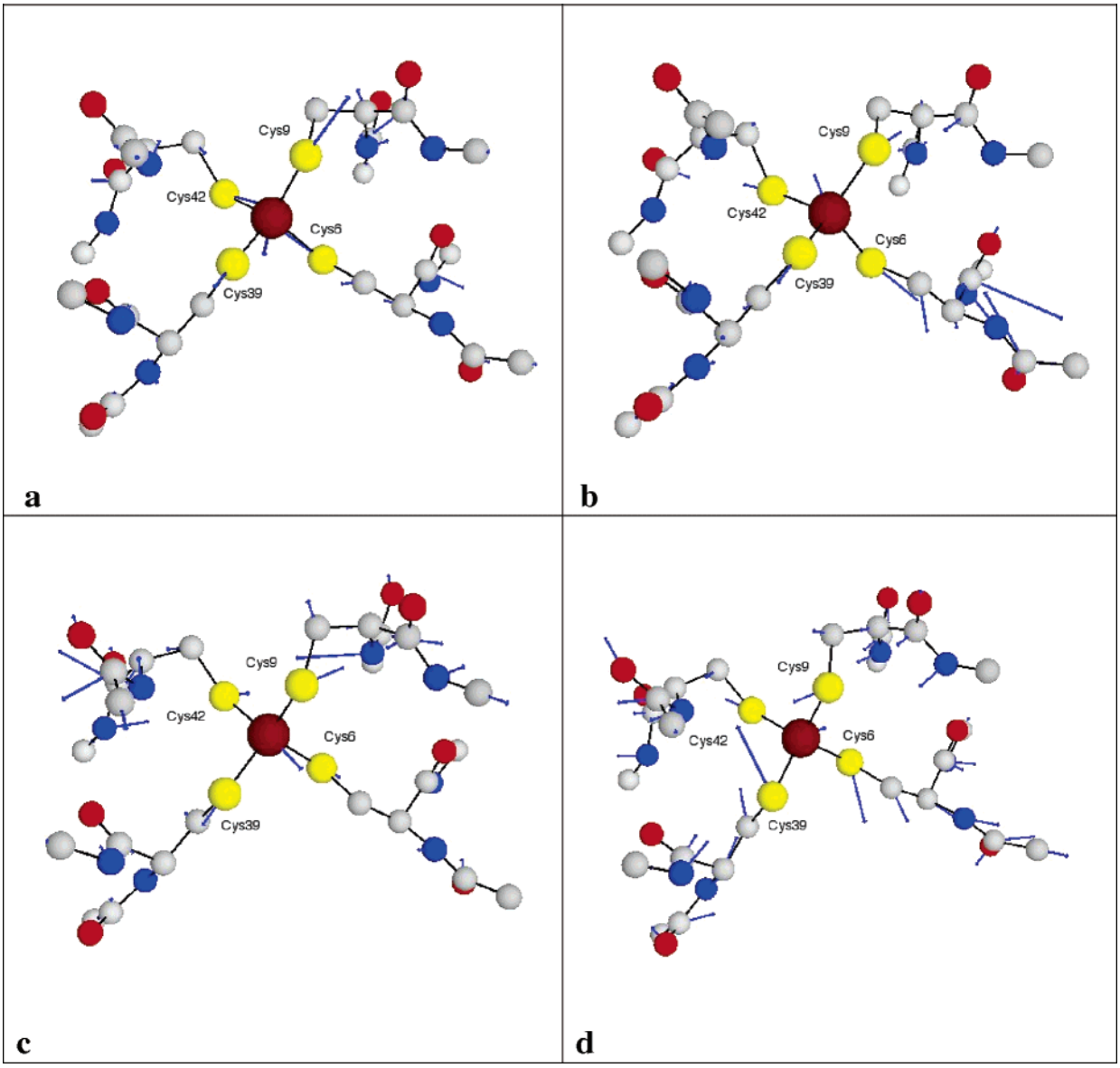


***Figure 4.*** Relative atomic motion involved in Rd normal modes. (a) 375 $cm^{-1}$; (b) 313 $cm^{-1}$; (c) 276 $cm^{-1}$; and (d) 66 $cm^{-1}$. Arrows have been rescaled between frames to enhance visibility.

3). Slightly weaker modes are calculated at 365, 363, and 340 $cm^{-1}$, and the combination of all these modes creates the broad envelope between 345 and 375 $cm^{-1}$. At lower frequencies, in the symmetric stretch or "breathing" region, the simulation exhibits three components at 337, 325, and 313 $cm^{-1}$. For comparison, resonance Raman features are seen at 333, 325 $cm^{-1}$ and at 313 $cm^{-1}$. Although these breathing modes are strongly enhanced in the Raman, they have much less Fe motion than the asymmetric Fe−S stretches, as shown in Figure 4; hence they have about 10% of the NRVS intensity as the asymmetric stretches. Along with S−C−C bending motion, a relatively large contribution to the PED of these modes comes from C−C−N, C−C−C, and C−N−C bending; this will be discussed further below.

The region with NRVS intensity near 150 $cm^{-1}$ involves S−Fe−S bending modes. It can be seen from Tables S1 and S2 and Figure 3 that S−Fe−S bending is strongly mixed with combinations of other bending motions. The Fe(S-cys$X_5$)$_4$ model predicts a cluster of modes near 150 $cm^{-1}$; these can be viewed as derived from the original triply degenerate $T_2$ bend modes. Furthermore, there is considerable NRVS signal between 140 and 340 $cm^{-1}$; the PVDOS does not return to baseline. This is in sharp contrast with recent results on the tetrahedral model system $FeCl_4^-$, which exhibits essentially zero intensity between 160 and 360 $cm^{-1}$.[50] In the simulation, this intensity is partially explained by additional groups of modes with centroids at 125, 170, 190, and 270 $cm^{-1}$. Previously, Raman features at 174 and 184 $cm^{-1}$ were assigned primarily to Fe−S−C bending[22] or a mix of S−Fe−S and Fe−S−C bending.[23] We note that our force field reproduces the bending region frequencies more accurately than previous models that were optimized primarily for the stretch region.

The lowest frequency modes, below 100 $cm^{-1}$, have never been seen before in rubredoxin. In our model, these modes involve concerted in-phase motion of entire cysteine residues

(50) Smith, M. C.; Xiao, Y.; Wang, H.; Coucovanis, D.; Koutmos, M.; Sturhahn, W.; Alp, E. E.; Zhao, J.; Yoda, Y.; George, S. J.; Cramer, S. P. *Inorg. Chem.* **2005**, *44*, 5562−5570.

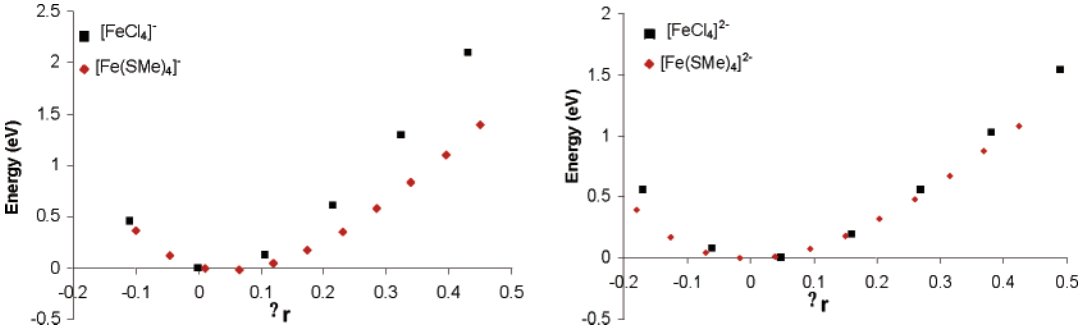


***Figure 5.*** Potential energy surfaces as a function of Fe−X distance derived from DFT calculations for (left) $[FeCl_4]^-$ and $[Fe(SMe)_4]^-$ and (right) $[FeCl_4]^{2-}$ and $[Fe(SMe)_4]^{2-}$.

***Table 2.*** Comparison of DFT Calculations with Experimental Values

| | Fe-X bond lengths (Å) | | frequency ($cm^{-1}$) expt | | frequency ($cm^{-1}$) calcd | | force constants(mdyne/Å) | ligand–metal bond covalency | bond dissociation energy (kcal/mol) |
|---|---|---|---|---|---|---|---|---|---|
| | expt | calcd | $T_2$ | $A_1$ | $T_2$ | $A_1$ | | | |
| $[Fe(SMe)_4]^-$ | 2.29 | 2.34 | 360 | 310 | 327 | 288 | 1.27 | 38.75 | −1403.71 |
| $[Fe(SMe)_4]^{2-}$ | 2.36 | 2.41 | 300 | | 250 | | 0.86 | 21 | −641.785 |
| $[FeCl_4]^-$ | 2.18 | 2.24 | 378 | 340 | 361 | 314 | 1.51 | 22 | −1383.37 |
| $[FeCl_4]^{2-}$ | 2.28 | 2.39 | 286 | | 230 | | 0.83 | 9 | −625.668 |

(Figure 4); in the protein, they would presumably correspond to collective motion of large segments of polypeptide. Modes between 20 and 80 $cm^{-1}$ have been seen with femtosecond pump−probe techniques[51] and inelastic neutron scattering[52] in blue Cu proteins such as azurin and plastocyanin, which are of comparable size. In these proteins, they have been referred to as "phononlike"[53] or as "delocalized mode(s) involving the protein skeleton motion".[54] Similar modes have also been seen in heme proteins by NRVS[55] and inelastic neutron scattering.[56,57]

**Reduced Rd.** The analysis for reduced *Pf* Rd followed the same lines used for the oxidized sample. For the reduced protein, in the $Fe(S\text{-}cysX_5)_4$ model, the Fe−S stretch force constant is lower by 31%, from 1.24 down to 0.92 mdyn/Å to account in part for the 65 $cm^{-1}$ (∼18%) shift of the asymmetric Fe−S stretching band. This is the first time that an experimentally derived Fe−S stretch force constant has become available for reduced rubredoxin. (A 30% reduction of $K_{Fe-S}$ was inferred for the Fe(II) site in 2-Fe ferredoxins from the resonance Raman of the mixed valent form.[58]) In contrast, the main bending peak stays nearly the same in the reduced vs oxidized Rd NRVS (166 vs. 172 $cm^{-1}$), hence it is not surprising that the S−Fe−S bend force constant $H_{SFeS}$ changes very little, from 0.18 mdyne/Å to 0.15 mdyne/Å.

One consequence of the weaker Fe−S stretching force constant for the reduced species is stronger coupling of Fe−S stretching modes with ligand bending and torsion motion. For example, in the region around 270 $cm^{-1}$ derived from the symmetric Fe−S stretch, the calculated PVDOS exhibits a resolved peak instead of the shoulder in the oxidized NRVS. This extra intensity is confirmed in the experimental data. Overall, there is significantly more intensity between 150 and 300 $cm^{-1}$ for the reduced form, indicating that Fe motion is coupled to a wider range of modes in the reduced protein.

**DFT Calculations.** From the experimental spectra, the metal−ligand stretching force constant decreases ∼31% upon reduction of rubredoxin. This suggests that the bond is weakened considerably in the reduced state. The smaller Fe−S force constant for reduced Rd is consistent with the longer Fe−S bond length, but both quantities change less than might be expected. For comparison, using the decrease in $\nu_3$ upon reduction of $Fe^{III}Cl_4^-$ to $Fe^{II}Cl_4^{2-}$, from 378 to 286 $cm^{-1}$, the Urey−Bradley stretching constant $K_{Fe-Cl}$ was reported to decrease by 45%, from 1.51 to 0.83 mdyn/Å.[59] Similarly, the best estimate from EXAFS for the change in average Fe−S bond length for *Pf* Rd is 0.05 Å (2.29 vs. 2.34 Å),[17] while, in the $FeCl_4^{-,2-}$ pair, the change is more than twice as large: $Fe^{III}$−Cl 2.18 Å[60] vs $Fe^{II}$−Cl 2.29 Å. These observations are corroborated by ligand K-edge studies of the model complexes $[FeCl_4]^{-/2-}$ and $[Fe(SPh)_4]^{-/2-}$, where it is clearly seen that the ligand−metal bond covalency decreases from 155% to 84% for thiolate complexes and from 82% to 36% for chloride model complexes.[61] We have used spin unrestricted DFT calculations on $FeCl_4^{-,2-}$ and $[Fe(S\text{-}Me)_4]^{-/2-}$ pairs to better understand the different magnitudes of these force constant and bond strength changes.

The DFT calculations reproduce the observed trends in experimental bond lengths and frequencies very well (Table 2). Furthermore, the results indicate that the gas-phase bonding energy of the thiolate complexes is 4−5 kcal/mol/bond higher than the corresponding chloride complexes with the same Fe oxidation states. This indicates that the Fe−S bond has a weaker force constant but higher bond energy. However, a higher force constant is generally correlated with higher bond energy.

(51) Cimei, T.; Bizzarri, A. R.; Cerullo, G.; Silvestri, S. D.; Cannistraro, S. *Biophys. Chem.* **2003**, *106*, 221−231.
(52) Bizzarri, A. R.; Paciaroni, A.; Arcangeli, C.; Cannistraro, S. *Eur. J. Biophys.* **2001**, *30*, 443−449.
(53) Book, L. D.; Arnett, D. C.; Hu, H.; Scherer, N. F. *J. Phys. Chem. A* **1998**, *102*, 4350−4359.
(54) Nakashima, S.; Nagasawa, Y.; Seike, K.; Okada, T.; Sato, M.; Kohzuma, T. *Chem. Phys. Lett.* **2000**, *331*, 396−402.
(55) Sage, J. T.; Durbin, S. M.; Sturhahn, W.; Wharton, D. C.; Champion, P. M.; Hession, P.; Sutter, J.; Alp, E. E. *Phys. Rev. Lett.* **2001**, *86*, 4966−4969.
(56) Doster, W.; Cusack, S.; Petry, W. *Nature* **1989**, *337*, 754−756.
(57) Cusack, S.; Doster, W. *Biophys. J.* **1990**, *58*, 243−251.
(58) Han, S.; Czernuszewicz, R. S.; Kimura, T.; Adams, M. W. W.; Spiro, T. G. *J. Am. Chem. Soc.* **1989**, *111*, 3505−3511.
(59) Avery, J. S.; Burbridge, C. D.; Goodgame, D. M. L. *Spectrochem. Acta* **1968**, *24A*, 1721−1726.
(60) Kistenmacher, T. J.; Stucky, G. D. *Inorg. Chem.* **1968**, *10*, 2150−2155.
(61) Glaser, T.; Rose, K.; Shadle, S. E.; Hedman, B.; Hodgson, K. O.; Solomon, E. I. *J. Am. Chem. Soc.* **2001**, *123*, 442−454.

To understand the above observation, potential energy surface (PES) calculations on these molecules were performed to investigate the change in bond energy along the $A_1$ stretching mode (Figure 5). The PES of the oxidized molecules (Figure 5) shows that the curvature (force constant) is higher for the Fe−Cl bond, as observed experimentally. These calculations also indicate that the covalency of the ligand−metal bond (in both Fe−Cl and Fe−S) does not change significantly even after stretching the bond by 0.2−0.3 Å. This implies that the covalent contribution to bonding energy is not responsible for the difference observed in the PES. The ionic contribution to the bond goes as $1/r$ and should be sensitive to changes in bond length. Since the covalent character for the Cls is less than that for the thiolates (Table 2), the effect there is large and should have a major contribution to the difference in force constant ($dV/dr$). Similar calculations on the reduced complexes indicate that the PESs are almost identical (Table 2) correlating with the similar force constants observed experimentally.

## Discussion and Conclusions

As a technique that is sensitive to $^{57}$Fe motion, NRVS provides a unique view of Fe−S protein dynamics. For oxidized Rd, the derived PVDOS complements the resonance Raman spectra. Additional modes are seen that are difficult to observe by Raman, including strong features below 100 cm$^{-1}$. Furthermore, the reduced protein is equally accessible to the NRVS method. A final special feature of NRVS is the potential for accurate intensity calculations; the amplitude of NRVS features reveals the fraction of kinetic energy due to Fe motion in a particular normal mode.

As illustrated in Figure 3, progressively more complex models for the environment of Fe in oxidized or reduced rubredoxin produce better simulations of the $^{57}$Fe PVDOS. A simple $D_{2d}$ Fe(SC)$_4$ model predicts a division of the spectrum into asymmetric Fe−S stretch, S−Fe−S/Fe−S−C bend, and S−Fe−S−C torsion regions, but at least a $C_1$ Fe(SCC)$_4$ model is needed to reproduce the splitting of the asymmetric stretch region and to capture some of the features between 150 and 350 cm$^{-1}$. Our results are thus in qualitative agreement with previous models based solely on Raman data. However, by including the complete cysteine residues in a more complex model, we obtained more quantitative agreement with the amplitudes in the bending region, as well as better reproduction of the PVDOS envelope in the 360 cm$^{-1}$ region. As expected, this model yields more NRVS intensity in the low-frequency region below 100 cm$^{-1}$ and a much better fit overall. One consequence of this more complex model is that the PEDs of most eigenvectors becomes mixed over a large number of internal coordinates (Figure 3 and Tables S1 and S2).

One issue that NRVS can address is the nature of "Fe−S" normal modes seen in resonance Raman spectroscopy. Czernuszewicz et al. have shown that kinematic interactions with S−C−C bend ($\delta_{SCC}$) can alter Fe−S stretching frequencies in rubredoxins.[23] As shown in Chart 1, in *Pf* Rd two of the FeS−CC dihedral angles are ∼90°, while the other two are ∼180°.[10,14] Czernuszewicz et al. highlighted the latter as key to the dynamics of Rd; they proposed that when the FeS−CC unit is nearly planar, the SCC bending modes mix strongly with Fe−S modes. As a consequence, two modes occur above the "natural" symmetric stretch $\nu_1$, at 314 and 324 cm$^{-1}$, while two modes were predicted to occur below $\nu_1$, at 244 and 273 cm$^{-1}$. Significant mixing also occurs for the three asymmetric stretch $\nu_3$ components. The importance of interacting Fe−S stretching and S−C−C bending modes and the influence of the Fe−S−C−C dihedral angle ($\tau$) were also highlighted in studies of $Fe_2S_2$(SR)$_2$ model complexes[62] and 2-Fe ferredoxins.[58] In contrast, Saito and co-workers have argued that, in rubredoxin, there is "extensive coupling between the Fe−S stretching and skeletal deformations around the FeS4 core".[24] Significant "kinematic coupling of the Fe−S stretch with deformations of the cysteine backbone, including the amide nitrogen conclusions," has also been deduced from the 1−2 cm$^{-1}$ shifts that arise from $^{15}$N-labeling of the cysteine nitrogens.[63]

In our analysis, to correctly reproduce the high frequency $^{57}$Fe PVDOS amplitudes, we found it necessary to include approximately five additional atoms (in each direction) beyond the ligating cysteine sulfurs. By a very different methodology, Qiu and co-workers also arrived at six-atom chains for their "chromophore-in-protein" model of blue copper sites.[49] Bending motions in these chains contribute to the nominal Fe−S stretching modes, as illustrated in Figure 4; this can also be seen in the PEDs in Figure 3 and Tables S1 and S2. In the Fe(S-cys$X_5$)$_4$ model, the asymmetric Fe−S stretch modes are as much as 66% Fe−S stretch in their potential energy distribution. For the remaining modes, all of the eigenvectors involve significant contributions from several internal coordinates.

Apart from shedding light on the composition of nominal Fe−S stretching modes, and quantification of the force constants in the reduced system, NRVS offers additional data about the appropriate parameters for the Fe-based bending and torsional motions. We note that many of the predicted bending frequencies deviate by 20−40 cm$^{-1}$ with previous force fields,[23] and some of the more recent studies do not even attempt low-frequency simulation.[64] Finally, we note that even our Fe(S-cys$X_5$)$_4$ model could not capture all of the observed intensity in the region below 100 cm$^{-1}$. Some of these low frequency modes presumably involve motion of large segments of the polypeptide chain, and additional work is needed on calculations that involve the entire Rd protein molecule.

Parametrized normal mode analysis of vibrational spectra is often a severely underdetermined problem. In some respects, every scientist conducting measurements regarding molecular dynamics is like one of the proverbial blind men studying an elephant; no technique gives the entire picture. The NRVS technique provides another point of view for our myopic spectroscopist. It has special strengths for observation of low-frequency large-scale protein modes, some of which may be important in the electron-transfer process. The information provided by NRVS also yields new data on the amplitudes of Fe motion in particular normal modes, as well as less stringent selection rules for normal modes in general. With the continuing development of even brighter synchrotron sources, NRVS

(62) Han, S.; Czernuszewicz, R. S.; Spiro, T. G. *J. Am. Chem. Soc.* **1989**, *111*, 3496−3504.
(63) Rotsaert, F. A.; Pikus, J. D.; Fox, B. G.; Markley, J. L.; Sanders-Loehr, J. *J. Biol. Inorg. Chem.* **2003**, *8*, 318−326.
(64) Kern, A.; Nather, C.; Studt, F.; Tuczek, F. *Inorg. Chem.* **2004**, *43*, 5003−5010.

should become a more routine technique that complements resonance Raman and infrared probes of biomolecular dynamics.

**Acknowledgment.** This work was funded by NIH GM-44380 (S.P.C.), GM-65440 (S.P.C.), GM-60329 (M.W.W.A.), NSF CHE-9980549 (E.I.S.) and the DOE Office of Biological and Environmental Research (S.P.C.). Use of the APS is supported by the DOE Office of Basic Energy Sciences, Office of Science. SPring-8 is funded by JASRI.

**Supporting Information Available:** Summary tables of NRVS and normal mode analysis for oxidized and reduced *Pyrococcus furiosus* rubredoxin and figures illustrating background subtraction process for oxidized and reduced rubredoxin. This material is available free of charge via the Internet at http://pubs.acs.org.

JA042960H